

# Energy Disposal in the $O(^3P) + \text{HCl}$ Reaction: Classical Dynamics and Comparison to Experiment

B. Ramachandran

Chemistry, College of Engineering and Science, Louisiana Tech University, Ruston, LA 71272, USA

The energy disposal in the  $O(^3P) + \text{HCl}(v = 2, j = 1, 6, 9) \rightarrow \text{OH}(v', j') + \text{Cl}$  reaction is analyzed using the results of fairly extensive quasiclassical trajectory (QCT) calculations on a realistic potential energy surface for the  $^3A''$  state of this system. These results are compared to the experimental observations of Zhang *et al.* [R. Zhang, W. J. van der Zande, M. J. Bronikowski, and R. N. Zare, *J. Chem. Phys.* **94**, 2704 (1991)]. The experimental and QCT product rotational distributions in the OH ( $v' = 1$ ) manifold,  $P_1(j')$ , are shown to be very similar in shape, but not magnitude, to the purely statistical “prior” distribution. On the other hand, the rotational distributions in the ground vibrational state of OH,  $P_0(j')$ , show significant deviations from prior distributions. A careful examination of several reactive trajectories suggests that (a) a direct abstraction mechanism is responsible populating the  $v' = 1$  states, (b) secondary encounters with  $R_{\text{HCl}} \leq R_{\text{HCl}}^\ddagger$  and  $\theta_{\text{OHCl}} > 100^\circ$  are responsible for populating the  $v' = 0, j' \geq 11$  states, and (c) secondary encounters with  $R_{\text{HCl}} \geq R_{\text{HCl}}^\ddagger$  and  $\theta_{\text{OHCl}} \leq 100^\circ$  may be responsible for populating the  $v' = 0, j' < 11$  states. The last observation raises the speculative but intriguing possibility that the state  $v' = 0, j' = 11$  may represent a phase space boundary between the two types of secondary encounters.

## I. INTRODUCTION

The correlation between the topology of potential energy surfaces for reactive systems and the energy disposal among the products has been a subject of historical interest in chemical reaction dynamics. From the early and pioneering studies of Polanyi and coworkers [1,2] and later investigations [3–5], a number of trends or propensity rules that govern energy disposal have been identified. For example, the role of reagent translational and vibrational energy in determining the product energy disposal in the case of atom + molecule reactions with “early” and “late” barriers is now well-accepted. Until recently, however, there was no *experimental* way to probe, in detail, the effect of reagent rotation on the partitioning of energy among the product degrees of freedom because of the difficulty in selecting and *systematically changing* the reagent rovibrational state. This has been accomplished by the research group of Zare in the last decade for the  $O(^3P) + \text{HCl}$  reaction [6,7], whereby the integral cross-sections for  $O(^3P) + \text{HCl}(v = 2; j = 1, 6, 9) \rightarrow \text{OH}(v' = 0, 1; j') + \text{Cl}$  are now available [8].

On the theoretical side, a new potential energy surface for this reaction, based on scaled *ab initio* energies at the MR-CISD+Q/cc-pVTZ level of theory (called the S4 surface), was recently obtained by the author and coworkers [9]. Quasiclassical trajectory (QCT) calculations on the S4 surface has reproduced many of the experimental observations. Moreover, thermal rate coefficient calculations on this surface using variational transition state theory [10] with multidimensional tunneling corrections [11] have yielded excellent agreement with available experimental data over a wide temperature range [12]. At the same time, recent calculations [13–18] have also brought

to light the deficiencies of the first *ab initio* surface to become available for this reaction, due to Koizumi, Schatz, and Gordon (KSG) [19]. Based on these reports, the S4 surface appears to be a more realistic representation of the lowest  $^3A''$  state of the  $O(^3P) + \text{HCl}$  system than earlier potential surfaces based on *ab initio* calculations [15,19–21]. Therefore, it is now possible to not only compare theoretical predictions of energy disposal with experimental results in this case, but also to examine the dynamical mechanisms at work in bringing about those outcomes. Such an inquiry is the subject of this paper.

There are three points of interest in the present study. One is that the experimental results show a near equipartitioning of energy in all degrees of freedom in the products *regardless* of the rotational state of HCl, in sharp contrast to the initial conditions and contrary to the expected conservation of both orbital and rotational angular momenta in  $H - L - H'$  type reactions [4,22]. The second is the experimentally observed vibrational branching leading to significant amounts of OH ( $v' = 0$ ) in addition to the energetically more favorable OH ( $v' = 1$ ). The production of OH ( $v' = 0$ ) is noteworthy because of the rather large amount of vibrational energy being redistributed, especially in view of the vibrational adiabaticity generally observed in  $H - L - H'$  type reactions [1–5,22] and the fact that no OH ( $v' = 0$ ) was observed in the chemically similar  $O(^3P) + \text{HBr}$  reaction [23]. The last point of interest is the shape of the OH ( $v' = 0$ ) rotational distributions,  $P_0(j')$ , obtained from HCl ( $v = 2, j = 1, 6$ ). The experimental distributions clearly show a non-monotonic rise in the  $P_0(j')$  in both cases, with a smooth rise up to  $j' = 10$  followed by pronounced dip at  $j' = 11$ . The distributions resume their monotonic rise from  $j' = 12$  onwards until  $j' = 15$  and 16, respectively, where the

distributions reach their maximum values. QCT calculations on the S4 surface [9] were able to account for the dip at  $j' = 11$  in the case of the HCl ( $v = 2, j = 1$ ) state and provided hints that a similar behavior may be present in the case of the (2, 6) state as well.

It should be noted that a completely quantum mechanical treatment of this reaction to obtain product rotational distributions that can be directly compared to experimental results remains a formidable challenge. Common approximations employed, such as the  $J$ -shifting method [19] or the extended constant centrifugal potential approximation (CCPA) of Nakamura *et al.* [24], do permit reliable estimates of the quantum rate coefficients, but are of dubious value in predicting product rotational distributions. On the other hand, the work of Aoiz and coworkers [25–29] has shown that, with sufficiently large ensembles of trajectories, the QCT method can reproduce many of the details of the quantum mechanical calculations, especially when threshold effects are not important. The reactions studied in the Zare experiments occur at energies well above the reaction barrier and are, therefore, likely to be essentially free from such quantum mechanical effects.

It is important, for the sake of completeness, to consider the relative importance of the  $^3A'$  electronic state in this reaction. This state is degenerate with the  $^3A''$  electronic state at collinear and asymptotic configurations of the three atom system but lies above it elsewhere. This means that the minimum energy saddle point energy on the  $^3A'$  surface is about 3.2 kcal/mol higher than the bent transition state on the  $^3A''$  (S4) surface [9]. Considerable evidence indicates that the role of the  $^3A'$  state may be neglected without loss of accuracy. For example, recent quantum mechanical calculations of thermal rate coefficients [13–15, 17, 18] have shown that the contributions from the  $^3A'$  electronic state must be small enough to be negligible except at extremely high temperatures. Our own recent QCT calculations [30] on a model of the  $^3A'$  state [31] indicate that contributions from this electronic state to the QCT product rotational distributions arising from HCl ( $v = 2; j$ ) are also vanishingly small.

The remainder of this paper is organized as follows. In Section 2, we present the details of the energy disposal analysis and compare the QCT results with the experimental results. We also compare the experimental and QCT rotational distributions to the “prior” distributions [32] calculated from purely statistical considerations. In Section 3, we examine the behavior of several reactive trajectories to study the detailed dynamics of the reaction. We conclude in Section 4 with a discussion of this work and its implications.

## II. ENERGETICS OF THE REACTION

The reaction of O( $^3P$ ) with HCl is almost thermoneutral, with  $\Delta H_0^\circ \simeq 0.95$  kcal/mol. The endothermicity of the reaction is due to the higher zero point energy of the OH molecule which more than compensates for the slightly larger dissociation energy  $D_e$  for OH compared to HCl. In the absence of the zero point energy, the reaction is exothermic by  $-0.08$  kcal/mol. Figure 1 presents, on the left hand side, the six vibrotational energy levels of HCl studied in this work. The HCl molecules in the experiments of Zhang *et al.* [7] were prepared in the lowest three of these six states. The mean center of mass collision energy  $\langle E_{coll} \rangle = 3.2$  kcal/mol for O + HCl collisions estimated by Zhang *et al.* was based on the O atom velocity distribution resulting from NO<sub>2</sub> photolysis at a slightly different wavelength [33] than was used in their experiment (351 nm in Ref. [33] as opposed to 355 nm in Ref. [7]). A presumably more accurate estimate of the collision energy distribution was reported by Aoiz *et al.* in a recent study [18] using the results of NO<sub>2</sub> photolysis experiments at 355 nm [34], which became available after Ref. [7] was published. This collision energy distribution function yields a value of  $\langle E_{coll} \rangle = 2.76$  kcal/mol. The grey vertical bars on the left hand side of Fig. 1 indicate the FWHM of the collision energy distribution function and the symbols superimposed on these bars indicate the value of the total energy corresponding to  $\langle E_{coll} \rangle = 2.76$  kcal/mol, for the three states studied experimentally.

Figure 1 also shows the  $v' = 0, 1$  and 2 vibrotational states of the OH molecule on the right. We note, for later reference, that the OH ( $v' = 2$ ) states are accessible at this value of the collision energy only from the HCl ( $v = 2, j \geq 9$ ) states. In fact, the  $v' = 2$  states of OH were not experimentally detected even for the  $(v, j) = (2, 9)$  initial state. Therefore, the average vibrational energy of the products in each case studied by Zhang *et al.* is necessarily considerably lower than that of the reactants. The difference is, of course, channeled into product rotation and translation, which will be an important consideration in our discussion of the energy disposal in Section 4. In the current Section, we show that QCT statistics, analyzed in a manner that preserves the proper energetics of the reaction, can account for the observed energy disposal pattern.

The QCT results for the present analysis were obtained by propagating 10 000 trajectories from each initial state at several collision energies. A total of 270 000 trajectories were propagated from the HCl (2,1), 230 000 trajectories from the (2,6), and 280 000 trajectories from the (2,9) states, spanning collision energies from the (classical) reaction threshold to 11.0 kcal/mol [9]. In order to examine the trends in energy disposal when the OH ( $v' = 2$ ) states become energetically accessible, we also propagated 10 000 trajectories each at 7 collision ener-

gies in the range 1.5 - 4.5 kcal/mol at 0.5 kcal/mol intervals (total of 70 000 trajectories per initial state) from the three initial states HCl ( $v = 2, j = 12, 15, 20$ ). The mean collision energy of these ensembles of trajectories, weighted by the collision energy distribution function mentioned above, is nearly identical to that of the larger ensembles initiated from the HCl ( $v = 2, j = 1, 6, 9$ ) states.

Our intention here is to analyze both the QCT and the experimental results on as equal a footing as possible. We adopt the common convention of denoting vibrational, rotational, and translational energy by the letters  $V, R$ , and  $T$ , respectively. The total energies available to the reagents and products are defined respectively as

$$\begin{aligned} \langle E_{tot} \rangle &= \langle E_{coll} \rangle + E_{v,j}^{\text{HCl}} - E_{0,0}^{\text{HCl}}, \\ \langle E'_{tot} \rangle &= \langle E_{tot} \rangle - \Delta H_0^\circ. \end{aligned} \quad (1)$$

Denoting the number of reactive trajectories at a given collision energy as  $N_r(E_{coll})$ , we define the following quantities: (a) the average product vibrational energy as

$$\langle E_{V'} \rangle_{\text{QCT}} = \int dE_{coll} f(E_{coll}) \frac{1}{N_r(E_{coll})} \sum_{k=1}^{N_r(E_{coll})} E_{V',k}, \quad (2)$$

(b) the average product rotational energy as

$$\langle E_{R'} \rangle_{\text{QCT}} = \int dE_{coll} f(E_{coll}) \frac{1}{N_r(E_{coll})} \sum_{k=1}^{N_r(E_{coll})} E_{R',k}, \quad (3)$$

and (c) the average product translational energy as

$$\langle E_{T'} \rangle_{\text{QCT}} = \langle E'_{tot} \rangle - \langle E_{V'} \rangle_{\text{QCT}} - \langle E_{R'} \rangle_{\text{QCT}}. \quad (4)$$

In these equations, the collision energy distribution function,  $f(E_{coll})$ , is normalized such that

$$\int dE_{coll} f(E_{coll}) \simeq \sum_i f(E_{coll,i}) = 1,$$

and the integrals are evaluated as sums over discrete collision energies.

A few comments about the vibrational energies  $E_{V',k}$  used in Eq. (2) are now necessary. In order to assign the rovibrational state of the product diatomic, QCT methods usually start by dividing the total product energy into translational and internal energy. The rotational state of the diatomic is found by equating the rotational angular momentum to  $\sqrt{j'(j'+1)}\hbar$  [35] which yields a value for  $j'$  and, thus, a value for  $E_{R'}$ . The vibrational energy,  $E_{V'}$ , is found by subtracting  $E_{R'}$  from the total internal energy. The  $E_{V'}$  is then equated to a Dunham expansion to find  $v'$ , which is rounded to the nearest integer. Using the vibrational energy thus found in

the energy disposal analysis leads to two problems in the present case. The first is the absence of zero point energy in QCT calculations. This is usually unimportant if the reactant and product diatomics have widely differing classical dissociation energies  $D_e$  which will then account for most of the reaction enthalpy. However, as noted above, zero point energies are vital ingredients in determining the energetics in this reaction. The second is that since  $v'$  is a continuous variable, at least in the case of the  $\text{O}(^3P) + \text{HCl}$  reaction, the QCT calculation tends to overestimate the average vibrational energy at a given collision energy. For example, the average *actual* values of  $v'$  for the ground and first excited vibrational states of OH from QCT calculations are, respectively, 0.13 and 1.11. While these may not appear to be large deviations from the ‘‘correct’’ values of 0 and 1, it is essential to note that a deviation as small as 0.1 from the actual value in the  $v'$  quantum number in this case ( $\omega_e = 3737 \text{ cm}^{-1}$  or 10.69 kcal/mol) leads to a deviation greater than 1.0 kcal/mol in the calculated vibrational energy. We avoid both these difficulties by ‘‘quantizing’’ the vibrational energy by setting  $E_{V',k}(v') = (E_{v',0}^{\text{OH}} - E_{0,0}^{\text{OH}})$ , where the  $E_{v',j'}$  values are taken from the quantum mechanical energies presented in Fig. 1. Although the QCT rotational energies also similarly deviate from the quantized values, because of the smaller spacing between rotational levels, this does not have the same dramatic impact on the energy disposal analysis as in the case of the vibrational energy. Therefore, in Eq. (3), we use the actual rotational energy,  $E_{R'}$ , found by the trajectory code. Since the vibrational energy is adjusted in Eq. (2), it becomes necessary to calculate the translational energy using Eq. (4).

We also recalculate the experimental values for the average energies  $\langle E_{V'} \rangle$ ,  $\langle E_{R'} \rangle$  and  $\langle E_{T'} \rangle$  using the value of  $\langle E_{coll} \rangle = 2.76 \text{ kcal/mol}$ . These calculations follow the same procedures employed by Zhang *et al.*, and are based on the experimental product rotational distributions  $P_{v'}(j')$  taken from Ref. [7]. Thus, we obtain

$$\langle E_{V'} \rangle_{\text{Expt.}} = \frac{\sum_{v'} \sum_{j'} P_{v'}(j') (E_{v',0}^{\text{OH}} - E_{0,0}^{\text{OH}})}{\sum_{v'} \sum_{j'} P_{v'}(j')}, \quad (5)$$

$$\langle E_{R'} \rangle_{\text{Expt.}} = \frac{\sum_{v'} \sum_{j'} P_{v'}(j') [E_{v',j'}^{\text{OH}} - E_{v',0}^{\text{OH}}]}{\sum_{v'} \sum_{j'} P_{v'}(j')}, \quad (6)$$

and

$$\langle E_{T'} \rangle_{\text{Expt.}} = \langle E'_{tot} \rangle - \langle E_{V'} \rangle_{\text{Expt.}} - \langle E_{R'} \rangle_{\text{Expt.}}. \quad (7)$$

We further define, for both the QCT and experimental cases, the fractions

$$\begin{aligned} f_{V'} &= \langle E_{V'} \rangle / \langle E'_{tot} \rangle \\ f_{R'} &= \langle E_{R'} \rangle / \langle E'_{tot} \rangle \\ f_{T'} &= \langle E_{T'} \rangle / \langle E'_{tot} \rangle \end{aligned} \quad (8)$$

which traditionally form the basis for energy disposal analysis. The results of this analysis are presented in Fig. 2, where the black filled symbols represent the experimental values for the three initial states probed by Zhang *et al.* and the solid lines connecting empty symbols represent the QCT values for the six states examined above. Also shown, as dashed lines with smaller, grey-shaded symbols, are the reactant energy fractions  $f_V = E_V / \langle E_{tot} \rangle$ , etc., analogous to those in Eq. (8) for the products.

It is clear from Fig. 2 that the QCT and experimental fractions are in good agreement for all three types of energies, the agreement being slightly poor in the case of the HCl (2,1) state. The reason for the discrepancy in this case can be readily identified by comparing the QCT and experimental product rotational distributions (see Fig. 3 below) and the vibrational branching ratios, defined as the ratio of the collision energy averaged vibrationally resolved reactive cross sections  $\langle \sigma_{v'=1}^r \rangle / \langle \sigma_{v'=0}^r \rangle$  [9]. In this case, the QCT distribution in the OH ( $v' = 0$ ) manifold is a sharply peaked narrow distribution while the vibrational branching ratio of 4.30 is much higher than the experimental value of 2.7. The sharply peaked QCT rotational distribution lowers the value of  $\langle E_{R'} \rangle$  while the larger value of the vibrational branching ratio leads to a much larger value of  $\langle E_{V'} \rangle$ . However, these two errors mutually balance each other in Eq. (4) to yield a value of  $\langle E_{T'} \rangle$  in excellent agreement with experiment. As one may guess from Fig. 2, the QCT product rotational distributions and vibrational branching ratios for the (2,6) and (2,9) states of HCl (3.1 and 3.7, respectively [9]) are in much better agreement with the experimental results (3.0 and 4.1, respectively [7]). An important observation to be made from Fig. 2 is that the product energy disposal patterns show no sensitivity to the dramatic increase in the reagent rotational energy for the lower three initial states studied but begin to show somewhat weak trends for the higher three. We will return to this point in Section 4.

It is instructive to compare the experimental and QCT product rotational distributions to the “prior” distributions,  $P_{v'}^0(j')$ , calculated from purely statistical considerations. We use the definition [32]

$$P_{v'}^0(j') \propto (2j' + 1) [E_{tot}^i - (E_{v'j'} - E_{0,0})]^{1/2}. \quad (9)$$

Because of the spread in the collision energies in the experiments, the  $E_{tot}^i$  in Eq. (9) is calculated as the average of the absolute energies of the highest occupied  $E_{v'j'}$  level in the experimental distributions and the next highest one. So, for example, in determining  $E_{tot}^i$  for the distributions resulting from the HCl (2,1) state, we average the OH energy levels  $E_{1,13}^{\text{OH}}$ , the highest energy state populated, and  $E_{1,14}^{\text{OH}}$ , the next higher energy level. Normalizing these distributions in the same way as Zhang *et al.* (i.e., requiring  $\sum_{j'} P_0^0(j') + \sum_{j'} P_1^0(j') = 1$ ),

yields the vibrational branching ratios 0.51, 0.55, and 0.61 for  $j = 1, 6, 9$  which are, of course, in serious disagreement with the experimental results. Statistically, the OH ( $v' = 0$ ) manifold has a much higher probability of being populated than the  $v' = 1$ . The vibrational inversion observed in the experiments is, therefore, certainly a dynamical effect, commonly attributed to vibrational adiabaticity in light atom transfer reactions. Taking this effect into account by renormalizing the prior distributions so that  $\sum_{j'} P_{v'}^0(j') = \sum_{j'} P_{v'}^{\text{Expt}}(j')$  for each  $v'$  permits more illuminating comparisons of the rotational energy distributions within each vibrational level. These *renormalized* priors resulting from the HCl (2,1) initial state are compared to the experimental and QCT rotational distributions in Fig. 3.

It is clear from Fig. 3(a) that renormalized the  $P_1^0(j')$  distribution bears remarkable similarity to its experimental and QCT counterparts. Similar agreement between these distributions are found for the other two HCl initial states also. The  $P_0^0(j')$ , shown in Fig. 3(b) in contrast, is quite unlike the experimental and QCT distributions. Similar significant differences between these quantities are found in the other two cases as well. In the following Section, we examine the QCT dynamics of the reaction in some detail to understand the dynamical processes responsible for these outcomes.

### III. DYNAMICS OF THE REACTION

As a first step toward examining the detailed dynamics of the reaction, we sorted all reactive trajectories from a particular initial state by  $E_{coll}$ ,  $v'$ , and  $j'$ . About 100 trajectories from each of the three HCl initial states at collision energies close to  $\langle E_{coll} \rangle = 2.76$  kcal/mol were then chosen at random and examined and assigned to various groups. Below, we present and discuss the behavior of “typical” members of the dominant groups. It should be noted, however, that members of a certain group of trajectories are “typical” only in the sense that they are similar to each other in certain broad respects including the range of the rotational quantum number  $j'$ . Equally important also is the fact that clear differences in certain essential aspects can be identified between trajectories belonging to different groups.

We first examine the reactive trajectories that lead to OH ( $v' = 1$ ) rotational states. A typical trajectory that falls into this category is shown in Figure 4(a) at a collision energy of 3.0 kcal/mol. This trajectory clearly indicates a fast, direct abstraction of the H atom by the approaching O. The vibrational motion of the HCl remains remarkably free of any perturbative effects from the approaching oxygen atom almost up to the instant the oxygen makes “contact” with the H. Within less than a vibrational period after this, the new diatomic system has settled down to the vibrational motion of the OH.

The shift in the  $R^e$  value from 1.27 for HCl to 0.97 for OH is clearly visible. It is important to note that there is no hint of secondary encounters in this collision. Almost all the  $v' = 1$  trajectories we have examined display behavior qualitatively very similar to that shown in Fig. 4(a). A very small number of trajectories did show indications of secondary encounters, but these were rather “weak” in the sense that  $R_{\text{HCl}} > R_{\text{HCl}}^e$  after the primary encounter and there was no evidence of significant perturbations to the OH vibrational motion once the initial abstraction was over.

This raises the question of how the rotational distributions in the  $v' = 1$  levels become nearly statistical in nature. We believe that the answer lies in the topology of the potential energy surface in the saddle point region as well as the total energy available to the reagents. It is now well-established that the saddle point for this reaction lies at a bent geometry of the O-H-Cl system [9,19,20,15,36]. The minimum energy saddle point on the S4 surface corresponds to  $R_{\text{OH}}^\ddagger = 1.28\text{Å}$ ,  $R_{\text{HCl}}^\ddagger = 1.41\text{Å}$ , and  $\theta_{\text{OHCl}}^\ddagger = 131.4^\circ$  [9]. However, it is clear from Fig. 1 that the reagents have total energies far greater than the barrier height and, therefore, the direct abstraction of the H by O is possible over a rather wide range of  $\theta_{\text{OHCl}}$ , roughly  $100^\circ \leq \theta_{\text{OHCl}} \leq 180^\circ$ . At these angles, the repulsive energy release in the exit channel is efficiently channeled into product rotation and translation in what has been termed “mixed energy release” by Polanyi [1,2]. The precise partitioning of energy between the two degrees of freedom depends sensitively on (a) the angle of attack and (b) the vibrational phase of the HCl at the moment of “contact,” at least in the classical sense. Both of these are subject to fairly large variations from collision to collision. This may explain why the rotational distribution in the  $v' = 1$  states are similar to the prior distributions *in spite of* the direct abstraction mechanism which precludes any opportunity for energy randomization through a collision complex. This may also explain why a statistical algorithm, based on the assumption of a long-lived O-H-Cl complex, was able to predict  $v' = 1$  rotational distributions for this reaction in good agreement with the experimental observations [37].

We now examine the trajectories that lead to the OH( $v' = 0$ ) rotational states, a “typical” representative of which is presented in Figure 4(b), also at a collision energy of 3.0 kcal/mol. The differences between the trajectories plotted here and those of Fig. 4(a) are immediately obvious. In this case, even though the initial encounter between the O and HCl is similar to that of Fig. 4(a), there is evidence of strong secondary encounters that nearly regenerate the HCl molecule. Two characteristics of these trajectories account for the observed rotational excitation of the OH ( $v' = 0$ ) molecules. The first is that the vibrational amplitude of the OH formed after the primary encounter is quite large, indicating that  $v' > 0$ ,

and remains large until the secondary encounter. Second,  $R_{\text{ClO}}$  remains well above the equilibrium bond distance of 1.57 throughout the collision, indicating that the angle  $\theta_{\text{OHCl}}$  remains large while  $R_{\text{HCl}}$  approaches  $R_{\text{HCl}}^e$  at the instant of the secondary encounter. Such large-angle interactions of the OH with the Cl atom directs most of the vibrational energy present in the OH after the primary encounter, *and the repulsive energy release in the exit channel*, into the recoil of H from the Cl. Since the O is not directly repelled by the Cl, the light H atom ends up spinning rapidly around the relatively slowly departing oxygen atom. This accounts for the high degree of rotational excitation observed in the  $v' = 0$  manifold.

Excluded from the group of “typical” trajectories represented in Fig. 4(b) are those that form OH ( $v' = 0, j' \leq 10$ ) from HCl ( $v = 2, j = 1, 6$ ). These are of special interest because of the non-monotonic rise of the  $P_0(j')$  observed experimentally. Detailed examination of these trajectories reveal certain distinct characteristics. A typical member of this group is presented in Figure 5. In this Figure, we have also shown the bond angle  $\theta_{\text{OHCl}}$  as a function of time for easy reference. It is clear from Fig. 5 that like the trajectory pictured in Fig. 4(b), these trajectories also undergo secondary encounters after the abstraction of the H by the O. However, unlike the case in Fig. 4(b), these encounters typically take place with  $R_{\text{HCl}}$  larger than  $R_{\text{HCl}}^\ddagger$  but at rather small values of  $\theta_{\text{OHCl}}$ . In the particular instance shown in Fig. 5,  $\theta_{\text{OHCl}} = 96.5^\circ$  at the instant of the secondary encounter, which is marked by the filled circle in the Figure. These regions of configuration space are accessible on the S4 surface only in the exit channel (i.e.,  $R_{\text{HCl}} > R_{\text{HCl}}^\ddagger$ ) where a deep minimum is present at  $R_{\text{OH}} = 1.00$ ,  $R_{\text{HCl}} = 2.18$ , and  $\theta_{\text{OHCl}} = 80.4^\circ$  [9]. Since the system is in the exit channel, the H atom remains at some distance from the Cl and the repulsive energy release acts between the Cl and O, channeling more the energy into translational motion and considerably less into rotation. From our examination of this group of trajectories (i.e., those that lead to  $j' \leq 10$ ), it appears that  $\theta_{\text{OHCl}}$  at the instant of the secondary encounter is less than  $100^\circ$  in each case. On the other hand, we have verified that in each of the cases represented by Fig. 4(b), the bond angle at the instant of the secondary encounter is  $\geq 120^\circ$  [ $\theta_{\text{OHCl}} = 125.9^\circ$  in the particular case shown in Fig. 4(b)]. Based on this analysis, it appears that the  $v' = 0, j' = 11$  state of OH may define a phase space separatrix that separates the small angle encounters that populate the lower  $j'$  levels from the larger angle encounters that lead to rotational excitation. Although this would account for the “dip” in the  $P_0(j')$  at  $j' = 11$  (since it is hard to hit a separatrix “dead on”), it is essential to stress the speculative (and purely classical!) nature of this suggestion.

In the course of examining the reactive trajectories, we also encountered a few exceptionally long-lived three-

atom complexes that survive for a few *rotational* periods of the O-H-Cl system and slightly more numerous moderately long-lived complexes that survive for 4-8 vibrational periods of the OH. However, similar to the cases of secondary encounters in trajectories forming OH ( $v' = 1$ ), these were by far the exception rather than the rule thereby eliminating any possibility that this reaction may proceed through a long-lived complex. A small number of  $v' = 0$  trajectories were also found that showed no indication of secondary encounters. These trajectories invariably populated states with  $j' \geq 17$  in nearly isoergic  $V \rightarrow V' + R'$  transfers.

In the absence of reliable theoretical evidence at the time, Zhang *et al.* [7] did suggest the possibility that a bent transition state, repulsive energy release in the exit channel, and secondary encounters in the exit channel could account for the observed outcomes in this reaction. It is gratifying that the present theoretical study provides ample support to each of these conjectures. However, the theoretical evidence also shows that the (classical) dynamics of this reaction is far more complex than expected. In the following Section, we discuss and highlight a few of the important aspects of reaction dynamics that have come to light as a result of this work.

## IV. DISCUSSION

### A. Energy Disposal

One of the more intriguing observations from the experiments of Zhang *et al.* is that rotational excitation of the reagent molecule has almost no effect on the energy disposal in the products. Regardless of the initial reagent rotational state, their analysis shows a near-equipartition of energy among the vibrational, rotational and translational modes, with  $\langle E_{V'} \rangle$ ,  $\langle E_{R'} \rangle$ , and  $\langle E_{T'} \rangle$  all lying within  $\simeq 2$  kcal/mol of each other, an observation reproduced almost perfectly by the QCT calculations on the S4 surface. Although secondary encounters could “explain why the energy disposal in the O + HCl reaction has essentially no memory of the reagent rotation,” [7] one cannot rule out the possibility that the observed near-equipartition of energy is a consequence of the choice of initial conditions in the experiments. It is clear from Fig. 1 that the initial states selected and the collision energy available from NO<sub>2</sub> photolysis at 355 nm provide sufficient energy to populate only the  $v' = 0, 1$  states of OH in detectable amounts, which means that the remainder of the energy must be channeled into product rotation and translation. Since the  $v' = 0$  states make no contribution to  $\langle E_{V'} \rangle$ , the value in each case is indicative of the extent to which the  $v' = 1$  level is populated. The higher  $j'$  states in each vibrational level contribute significantly to  $\langle E_{R'} \rangle$  while the lower  $j'$  states necessarily make significant contributions to  $\langle E_{T'} \rangle$ . The inaccessibility of

the  $v' = 2$  states, the significant vibrational branching that diverts between 24 and 37% of the products to the  $v' = 0$  states, and the significant rotational excitation in the  $v' = 0$  levels, all combine to deposit approximately equal amounts of energy into the three modes of energy disposal available to the reaction. On the other hand, it is clear from Fig. 2 that when the energy of the initial states are high enough for the higher rotational states of the  $v' = 0, 1$  manifolds and the  $v' = 2$  manifold to be accessible, the  $f_{R'}$  begins to reflect the increase in  $f_R$ . Therefore, it is justifiable to speculate that if the experiments had probed, say,  $j = 10, 15$ , and 20, some effect of reagent rotation would have been observed in the product energy disposal. In spite of this comment, however, Fig. 2 largely bears out the conclusions of Zhang *et al.* in that over the extended range of  $j$  studied here, the product fractions  $f_{R'}$  and  $f_{V'}$  are remarkably insensitive to the large changes in the reagent fractions  $f_R$  and  $f_V$ .

### B. Role of Reagent Rotation

A specific role for reagent rotation in the outcome of the reaction even for the lower three initial states is, however, indicated by our analysis. This is manifested in the vibrational branching ratio  $\langle \sigma_{v'=1}^r \rangle / \langle \sigma_{v'=0}^r \rangle$ , found to be 2.7, 3.0 and 4.1 experimentally and 4.3, 3.1 and 3.7 from QCT calculations. The experiments show that this quantity increases with increasing  $j$ , and the QCT ratios for the  $j = 6$  and 9 states closely match the experimental values. Since secondary encounters appear to be responsible for populating the  $v' = 0$  states of OH, this implies that increasing rotational excitation of the reagent molecule inhibits secondary encounters. QCT calculations initiated from the three higher initial states support this hypothesis. The initial states HCl  $v = 2, j = 12, 15, 20$  yield vibrational branching ratios of 5.9, 7.1 and 5.0. The decrease in the ratio for  $j = 20$  could signal the inhibition of direct abstraction due to the rapid rotation of the reagent. Interestingly, the branching ratio  $\langle \sigma_{v'=2}^r \rangle / \langle \sigma_{v'=0}^r \rangle$  also shows a similar pattern. This ratio is 4.4, 5.9 and 4.6, respectively, for  $j = 12, 15, 20$ . Another observation, also reproduced by QCT calculations and suggestive of a role for reagent rotation in the outcome of the reaction, is the increase in the energy averaged reaction cross section  $\langle \sigma_{v,j} \rangle$  with increasing  $j$ . The ratio  $\langle \sigma_{2,9} \rangle / \langle \sigma_{2,1} \rangle$  is  $1.5 \pm 0.5$  experimentally [7] and 1.41 from QCT calculations [9]. Based on the present set of calculations, the QCT cross sections appear to continue their increase as  $j$  is increased, with  $\langle \sigma_{2,j} \rangle / \langle \sigma_{2,1} \rangle = 2.7, 4.0$ , and 4.70 for  $j = 12, 15$  and 20, respectively.

### C. Propensity Rules

The broad features of the experimental and QCT rotational distributions, such as the average magnitude, the range of  $j'$  spanned etc., are rather insensitive to the initial  $j$  state. This is in agreement with quantum reactive scattering calculations on the Cl + HCl reaction, another  $H-L-H$  system, by Schatz *et al.* [38–40]. It is clear from Fig. 3 that the renormalized prior distributions agree well with the experimental distributions for the  $v' = 1$  states. This was found to be true for the other two initial states studied in the experiment also, thus indicating that the rotational energy is distributed almost statistically among the  $v' = 1$  rotational states. On the other hand, the rotational distributions in the  $v' = 0$  manifold are much hotter than the prior distributions and show little variation with changing  $j$ . In Section 3, we have proposed dynamical mechanisms to explain these outcomes. The observations and the proposed mechanisms call into question the kinematic propensity rule in  $H-L-H'$  type reactions that predict the conservation of rotational and orbital angular momenta ( $j \rightarrow j'; l \rightarrow l'$ ) [4,22]. Interestingly, the calculations on the Cl + HCl reaction [38–41] were carried out on LEPS surfaces with collinear saddle points, thereby eliminating the possibility that only reactions passing through bent transition states may be the exception to this rule. Schatz *et al.* [38], and Aker and Fulmer [41] have noted that in these types of reactions, the forces exerted by the potential energy surface appear to have more influence than the mass-induced kinematic constraints which form the basis for the propensity rules. The dynamical mechanisms proposed above, which are clearly dependent on the topology of the potential energy surface, reinforce this conclusion. On the other hand, the analysis presented above does lend support to the  $V \rightarrow V'$  propensity rule [1–5,42], which accounts for the preferential population of the  $v' = 1$  state. Also, over the entire range of initial state rotational quantum numbers  $j$  studied in this work, there is evidence of  $R \rightarrow R'$  energy transfer although the net change in  $f_{R'}$  from the (2, 1) to the (2, 20) is only about 0.16 compared to a change of 0.39 for  $f_R$  over the same interval of  $j$ .

### D. Dynamics

The QCT analysis presented in the previous Section indicates that three types of dynamical processes are responsible for the observed product rotational distributions and vibrational branching ratios. The  $v' = 1$  states of the OH are formed predominantly through a direct abstraction mechanism in which the attack angle  $\theta_{\text{OHCl}}$  can sample a range of values in the interval  $100^\circ \leq \theta_{\text{OHCl}} \leq 180^\circ$ . Depending on the precise geometry and vibrational phase of the HCl during this encounter, varying amounts of energy is channeled into

product rotation, thereby leading to the almost statistical distribution of rotational energy among the  $v' = 1$  states. Secondary encounters of OH with the Cl atom with  $R_{\text{HCl}} \leq R_{\text{HCl}}^\ddagger$  appear to be responsible for the formation of the OH  $v' = 0, j' > 11$  states. Since the system remains at fairly large values of  $\theta_{\text{OHCl}}$  during this process, the repulsive energy release between the H and the Cl is effectively channeled into product rotation, thereby giving rise to rotational distributions that are much hotter than the statistical priors. In contrast, secondary encounters in the exit channel ( $R_{\text{HCl}} > R_{\text{HCl}}^\ddagger$ ) for  $\theta_{\text{OHCl}} < 100^\circ$  appear to be primarily responsible for populating the  $v' = 0$  states with  $j' < 11$ . At such small bond angles, the repulsive energy release operates between the relatively massive O and Cl atoms, channeling energy more efficiently into translation rather than rotation. A correlation between the range of angles accessible to the reaction at the saddle point and product rotational distributions have been observed for the Cl + HCl reaction also [39], where the use of a potential energy surface with a “tight” bending potential gave rise to colder rotational distributions.

The possibility of secondary encounters influencing energy disposal in  $H-L-H'$  type reactions has been recognized early on [1,2]. However, the present analysis is somewhat unique in that the dynamical mechanisms identified appear to be quite state-specific, i.e., direct abstraction to form  $v' = 1$  and secondary encounters to yield  $v' = 0$ . Although such state-specificity in dynamics may certainly exist in every reaction where similar conditions are present, to the best of our knowledge, this is the first instance of such a case being identified.

This study, however, has not been able to provide an unambiguous explanation for the rather unusual behavior of the  $P_0(j')$  resulting from HCl ( $v = 2, j = 1, 6$ ). It was conjectured above that the  $j' = 11$  state may represent a boundary or separatrix between the two types of secondary encounters identified here. The possibility of two dynamical mechanisms operating in a reaction to yield the same product has been recognized before, and has been termed “microscopic branching.” [2,43]. Interestingly, in such cases, bimodal distributions of the detailed rate coefficients  $k(v', j', T')$  as a function of  $j'$  for fixed  $v'$  have also been observed, as exemplified by the H + ClI reaction [43]. However, one cannot rule out the possibility that the relatively good agreement between experimental and QCT  $P_0(j')$  in the vicinity of  $j = 11$  is a fortunate coincidence, and the observed shape of  $P_0(j')$  could be due to purely quantum mechanical phenomena. For example, an important factor may be the *quantum* dynamics on the  $^3A'$  electronic state of OHCl which, as already mentioned in Section I, is degenerate with the  $^3A''$  at asymptotic and collinear configurations but lies above it elsewhere. Recent work by the author and coworkers [30] shows that, under the conditions present in the experiments, QCT reaction cross sections on the  $^3A'$  surface

[31] are vanishingly small for the HCl ( $v = 2, j = 1$ ) and more than an order of magnitude smaller than the corresponding  $^3A''$  cross sections for the (2, 6) and (2, 9) states. However, this does not rule out the possibility that quantum dynamics on this higher energy surface may be qualitatively different.

## V. ACKNOWLEDGMENTS

This research is supported in part by a grant to BR from the Louisiana Education Quality Support Fund, under contract no. LEQSF (1994-97)-RD-A-18 and the National Science Foundation, grant no. CHE 97-12764.

- 
- [1] J.C. Polanyi, *Acc. Chem. Res.* **5**, 161 (1972), and the references therein.
- [2] J.C. Polanyi, *Science* **236**, 680 (1987).
- [3] M. Kneba and J. Wolfrum, *Ann. Rev. Phys. Chem.* **31**, 47 (1980).
- [4] N. Sathyamurthy, *Chem. Rev.* **83**, 601 (1983).
- [5] I.W.M. Smith, *Acc. Chem. Res.* **23**, 101 (1990).
- [6] R. J. Rakestraw, K. G. McKendrick, and R. N. Zare, *J. Chem. Phys.* **87**, 7341 (1987).
- [7] R. Zhang, W. J. van der Zande, M. J. Bronikowski, and R. N. Zare, *J. Chem. Phys.* **94**, 2704 (1991).
- [8] We adopt the convention of using unprimed variables for reactants and primed ones for products.
- [9] B. Ramachandran, E.A. Schrader III, J. Senekowitsch, and R.E. Wyatt, *J. Chem. Phys.* **111**, 3862 (1999).
- [10] D.G. Truhlar, A.D. Issacson, and B.C. Garrett, in *Theory of Chemical Reaction Dynamics*, Ed., M. Baer (CRC Press, Boca Raton, FL, 1985), and references therein.
- [11] Y. -P. Liu, D. -h. Lu, A. González-Lafont, D. G. Truhlar, and B. C. Garrett, *J. Am. Chem. Soc.* **115**, 7806 (1993).
- [12] T.C. Allison, B. Ramachandran, D.G. Truhlar, and R.E. Wyatt, *J. Phys. Chem.* (to be submitted).
- [13] W.H. Thompson and W.H. Miller, *J. Chem. Phys.* **106**, 142 (1997); **107**, 2164 (1997).
- [14] B. Poirier, *J. Chem. Phys.* **108**, 5216 (1998).
- [15] T.C. Allison, B. Ramachandran, J. Senekowitsch, D.G. Truhlar, and R.E. Wyatt, *J. Mol. Struct. (Theochem)* **454**, 307 (1998).
- [16] B. Ramachandran, unpublished QCT calculations on various versions that preceded the S4 surface.
- [17] F. Matzkies and U. Manthe, *J. Chem. Phys.* **110**, 88 (1999).
- [18] F.J. Aoiz, L. Bañares, J.F. Castillo, M. Menéndez, and J.E. Verdasco, *PCCP* **1**, 1149 (1999).
- [19] H. Koizumi, G. C. Schatz and M. S. Gordon, *J. Chem. Phys.* **95**, 6421 (1991).
- [20] B. Ramachandran, J. Senekowitsch, and R.E. Wyatt, *Chem. Phys. Lett.* **270**, 387 (1997).
- [21] L. Wang, C. Kalyanaraman, and A.B. McCoy, *J. Chem. Phys.* **110**, 11221 (1999).
- [22] K. Schulten and R.G. Gordon, *J. Chem. Phys.* **64**, 2918 (1976).
- [23] K.G. McKendrick, D.J. Rakestraw, and R.N. Zare, *J. Phys. Chem.* **92**, 5530 (1988).
- [24] K. Nobusada, K. Moribayashi, and H. Nakamura, *J. Chem. Soc. Faraday Trans.*, **93**, 721 (1997).
- [25] F. J. Aoiz, V. J. Herrero, and V. Sáez Rábanos, *J. Phys. Chem.* **97**, 7423 (1992).
- [26] F. J. Aoiz, L. Bañares, V. J. Herrero, V. Sáez Rábanos, L. Schneider, and R. E. Wyatt, *J. Chem. Phys.* **101**, 5781 (1994).
- [27] L. Schnieder, K. Seekamp-Rahn, J. Borkowski, E. Wrede, K. H. Welge, F. J. Aoiz, L. Bañares, M. J. D'Mello, V. Sáez Rábanos, and R. E. Wyatt, *Science* **269**, 207 (1995).
- [28] F. J. Aoiz, L. Bañares, T. Diez-Rojo, V. J. Herrero, and V. Sáez Rábanos, *J. Phys. Chem.* **100**, 4071 (1996).
- [29] F. J. Aoiz, M. T. Martinez, M. Menéndez, V. Sáez Rábanos and J. E. Verdasco, *Chem. Phys. Lett.* **299**, 25 (1999).
- [30] B. Ramachandran, E.A. Schrader III, D. Adcock, and R.E. Wyatt (in preparation).
- [31] The extended LEPS model was used, where the three Sato parameters were obtained by fitting the collinear saddle point region of the S4 surface and a few MR-CISD+Q/cc-pVTZ energies for the  $^3A'$  state to represent the angular dependence of the potential at the saddle point.
- [32] R.D. Levine and R.B. Bernstein, *Molecular Reaction Dynamics and Chemical Reactivity* (Oxford, New York, 1987).
- [33] H. Zacharias, M. Geilhaupt, K. Meier, and K.H. Welge, *J. Chem. Phys.* **74**, 218 (1981).
- [34] V. P. Hradil, T. Suzuki, S. A. Hewitt, P. L. Houston, and B. J. Whitaker, *J. Chem. Phys.* **99**, 4455 (1993).
- [35] J. T. Muckerman and D. G. Truhlar, in *Atom-Molecule Collision Theory: A Guide to the Experimentalist*, Ed. R. B. Bernstein, Plenum, New York, 1979.
- [36] M.S. Gordon, K.K. Baldrige, D.E. Bernholdt, and R.J. Bartlett, *Chem. Phys. Lett.* **158**, 189 (1989).
- [37] P.A. Elofson and L. Holmlid, *Chem. Phys. Lett.* **166**, 112 (1990).
- [38] G.C. Schatz, B. Amaee, and J.N.L. Connor, *Chem. Phys. Lett.* **132**, 1 (1986).
- [39] G.C. Schatz, B. Amaee, and J.N.L. Connor, *J. Chem. Phys.* **92**, 4893 (1990).
- [40] G.C. Schatz, D. Sokolovski, and J.N.L. Connor, *Can. J. Chem.* **72**, 903 (1994).
- [41] P.M. Aker and J.P. Fulmer, *J. Chem. Phys.* **99**, 244 (1993).
- [42] Or, rather,  $\Delta V \rightarrow \Delta V'$ , which refers to the energy in excess of that required to surmount the barrier.
- [43] M.A. Nazar, J.C. Polanyi, and W.J. Skrlac, *Chem. Phys. Lett.* **29**, 473 (1974).

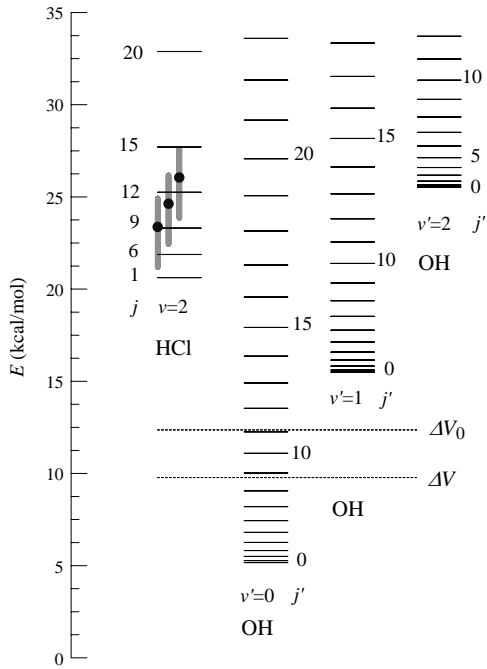


FIG. 1. Bound states of HCl and OH. The horizontal dashed lines represent the classical barrier height  $\Delta V$  and the vibrationally adiabatic barrier height  $\Delta V_0$ . The symbols and the gray vertical bars represent the estimated mean,  $\langle E_{coll} \rangle$ , and the range of collision energies, respectively, for the initial states probed in the experiments of Zhang *et al.* [7].

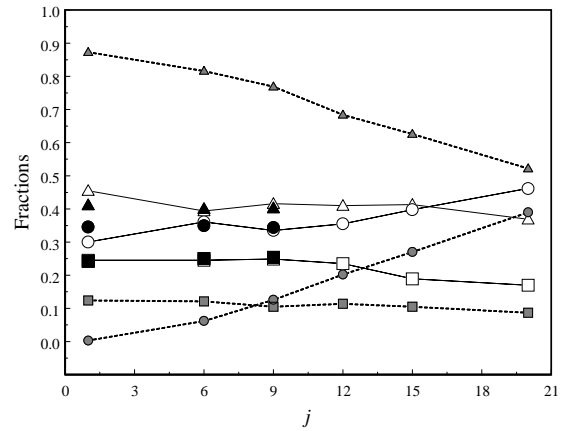


FIG. 2. Fractional energy in various modes of reactants and products as a function of the initial HCl rotational quantum number. Vibrational energy is represented as triangles, rotational energy by circles and translational energy by squares. The black filled symbols represent experimental data, and the empty symbols, the QCT data for products. The gray filled symbols represent reactant fractions.

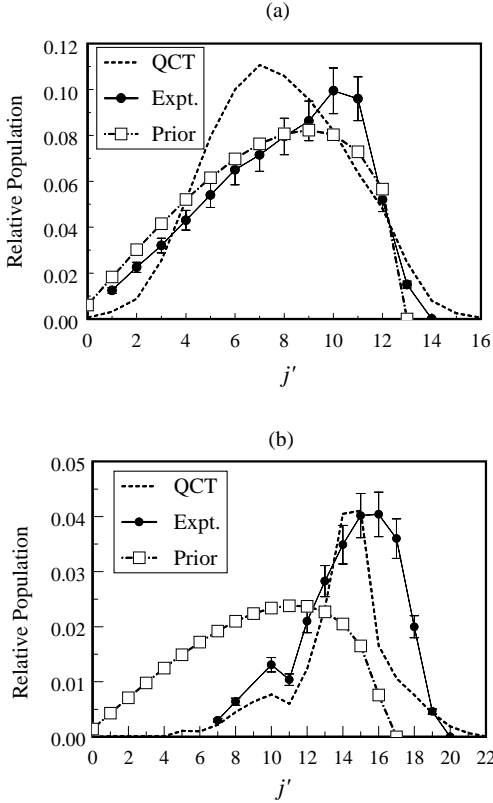


FIG. 3. Comparison of experimental, QCT, and prior rotational distributions of OH for reactions initiated in the HCl ( $v = 2, j = 1$ ) state. (a) Rotational distributions for OH ( $v' = 1$ ) and (b) for OH ( $v' = 0$ ).

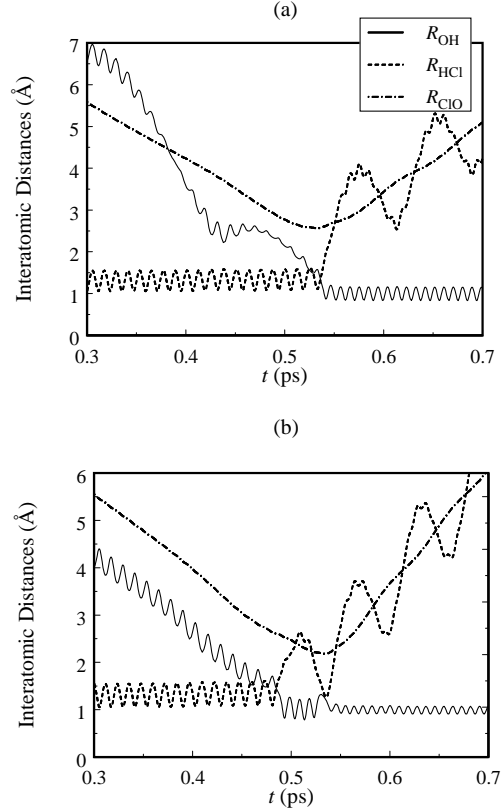


FIG. 4. Two types of “typical” reactive trajectories. (a) Direct abstraction of H from HCl ( $v = 2, j = 6$ ) to give OH ( $v' = 1, j' = 11$ ). (b) Abstraction of H from HCl ( $v = 2, j = 1$ ) followed by a secondary encounter to form OH ( $v' = 0, j' = 14$ ). Note that the vibrational amplitude of OH remains high between the primary and secondary collisions.

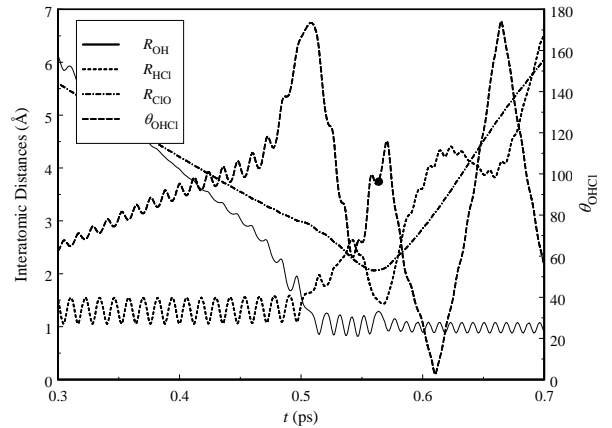


FIG. 5. A typical trajectory forming OH ( $v' = 0, j' < 11$ ). The bond angle  $\theta_{\text{OHCl}}$  refers to the right hand axis. The symbol marks the value of  $\theta_{\text{OHCl}}$  at the point of closest approach of the Cl and OH.